International Journal of Thermophysics, Vol. 23, No. 3, May 2002 (© 2002)

Thermophysical Properties of Nitrogen Trifluoride, Ethylene Oxide, and Trimethyl Gallium from Speed-of-Sound Measurements

J. J. Hurly[1]

Received November 28, 2001

The speed of sound was measured in gaseous nitrogen trifluoride, ethylene oxide, and trimethyl gallium using a highly precise acoustic resonance technique. The measurements span the temperature range 200 to 425 K and reach pressures up to the lesser of 1500 kPa or 80% of the sample vapor pressure. The speed-of-sound measurements have a relative standard uncertainty of less than 0.01%. The data were analyzed to obtain the constant-pressure ideal-gas heat capacity C_p^0 as a function of temperature with a relative standard uncertainty of 0.1%. The values of C_p^0 are in agreement with those determined from spectroscopic data. The speed-of-sound data were fitted by virial equations of state to obtain temperature-dependent density virial coefficients. Two virial coefficient models were employed, one based on square-well intermolecular potentials, and the second based on a hard-core Lennard-Jones intermolecular potential. The resulting virial equations reproduced the sound-speed data to within $\pm 0.02\%$, and may be used to calculate vapor densities with relative standard uncertainties of 0.1% or less.

KEY WORDS: C_2H_4O; ethylene oxide; equation of state; $Ga(CH_3)_3$; ideal-gas heat capacity; intermolecular potential; NF_3; nitrogen trifluoride; speed of sound; thermodynamic properties; trimethyl gallium; virial coefficients.

1. INTRODUCTION

Measurements of the speed of sound $u(T, p)$ in gaseous nitrogen trifluoride (NF_3), ethylene oxide (C_2H_4O), and trimethyl gallium ($Ga(CH_3)_3$) are reported. The measurements were made using a highly precise acoustic

[1] Process Measurements Division, Chemical Science and Technology Laboratory, National Institute of Standards and Technology, 100 Bureau Drive, Mail Stop 8363, Gaithersburg, Maryland 20899-8363, U.S.A. E-mail: john.hurly@nist.gov

0195-928X/02/0500-0667/0 © 2002 Plenum Publishing Corporation

resonance technique. The measured speeds of sound have uncertainties of $0.0001 \times u$. The sound speeds were collected along isotherms. The constant-pressure ideal-gas heat capacity $C_p^0(T)$ was determined for each isotherm with an uncertainty of $0.001 \times C_p^0$. The second $B(T)$ and third $C(T)$ virial coefficients were deduced for each species from the entire $u(T, p)$ surface. The densities $\rho(T, p)$ calculated from the virial equations of state have uncertainties of $0.001 \times \rho$.

These measurements are part of an ongoing program to determine the thermophysical properties of gases used in semiconductor processing. The data will be useful for modeling chemical vapor deposition (CVD) processes and will also provide a rational basis for the calibration of mass flow controllers (MFCs) which are used to meter these process gases.

2. EXPERIMENTAL TECHNIQUE

The speed-of-sound measurements reported in this manuscript were obtained using apparatus and experimental methods which have a documented history of high accuracy and reliability. The apparatus [1] and the acoustic model [2, 3] used to analyze the data are described in previous publications. Here, only a quick overview of the acoustic technique will be given.

The sample gas was contained in a cylindrical cavity (the resonator) that was approximately 14 cm long with a radius of 3.2 cm. The walls of the cavity were 1 cm thick monel (Alloy 400). The temperature-dependent dimensions of the resonator were accurately determined by calibration with argon, a gas for which the speed of sound is well known. The resonator was placed in a thermostated bath capable of maintaining a given temperature to within a few millikelvin. Two remote electro-acoustic transducers, maintained at room temperature, were connected by argon-filled waveguides to diaphragm flanges on the top of the resonator. The diaphragm flanges transmitted sound into and out of the resonator, and they separated the argon in the waveguides from the gas under study. One transducer was a speaker which generated sound that was transmitted through the waveguide into the resonator. The second transducer was a microphone which detected the sound transmitted through the resonator and the second waveguide.

The sample gas was allowed to reach equilibrium at a given temperature and pressure. The frequency f_{kns} and half-width g_{kns} were estimated for each resonance mode. (The modes were labeled with the subscripts "*kns*" used by Gillis [2].) This estimate required estimates of the gases' thermodynamic and transport properties. To precisely determine the resonance frequencies, the speaker scanned through 11 frequencies spanning twice the

estimated half-width centered on the estimated frequency. The amplitude and phase of the signal from the microphone were measured with a lock-in amplifier and recorded. The theoretically expected function for the shape of the resonance was then fitted to the amplitudes and phases to obtain improved values of f_{kns}, g_{kns} and their standard uncertainties. This process was then repeated with the 11 frequencies now spanning the improved values of f_{kns} and g_{kns} to obtain the final, accurate values of f_{kns} and g_{kns}. Typically, the standard deviation of $f_{k,n,s}$ from the fitting routine was less than $10^{-5} \times f_{k,n,s}$. An acoustic model of the cylinder [2, 3] was then used to correct the measured frequencies for viscous and thermal losses at the boundaries and for the fill duct used to move gas into and out of the resonator. These corrections also rely on estimates of the thermodynamic and transport properties of the sample gas. The sound speed was then calculated for each corrected resonance frequency from $u = 2\pi f_{k,n,s}/k_{k,n,s}$, where $k_{k,n,s}$ is the cylinder's wave number for the mode *kns* that was calculated from its known dimensions and eigenvalues.

Typically three frequencies were recorded at each temperature-pressure state. Two frequencies were for longitudinal modes; the third was for a radial mode. The three were averaged and used to estimate the weighted uncertainty in the tabulated speeds of sound.

3. RESULTS

3.1. Nitrogen Trifluoride, NF_3

Nitrogen trifluoride is a toxic gas that is used as a source of fluorine in plasma processes such as etching polysilicon, silicon nitride, tungsten silicide, and tungsten films, and for cleaning CVD chambers. The manufacturer designated the NF_3 "megaclass grade" with a purity of 99.996%, by volume. The speed of sound was measured at 323 states along 13 isotherms between 200 and 425 K. The six highest temperature isotherms were obtained using a pressure controller capable of operating up to 1.5 MPa. This pressure controller failed and was replaced with one that operated up to 1.0 MPa. Therefore, data at 300 K and lower temperatures extended up to only 1.0 MPa. Figure 1 shows the vapor pressure curve [4, 5] and the critical point of NF_3. The triple point temperature of NF_3 is approximately 66.46 K [6], and its critical parameters have been reported as $T_c = 510$ K [3], $P_c = 4.4$ MPa [5], and $\rho_c = 8.421$ kmol·m^{-3} [7]. The points on Fig. 1. show the states where the speed of sound was measured. The results for NF_3 are listed in Table I. At each temperature and pressure, two longitudinal and one radial mode were used to compute the tabulated values of the speed of sound. The weighted mean of these three values and their

Table I. Measured Speeds of Sound in Nitrogen Trifluoride

p (kPa)	u (m·s^{-1})	$10^6 \frac{\sigma[u]}{u}$
$T = 198.98$ K		
1004.0	155.028	70
943.9	156.101	64
872.6	157.342	62
805.4	158.484	56
742.1	159.532	56
673.3	160.649	47
589.7	161.969	46
532.9	162.848	51
465.3	163.880	59
421.2	164.537	63
373.4	165.244	65
310.8	166.154	74
259.9	166.887	86
210.3	167.592	85
149.1	168.448	90
100.0	169.131	88
$T = 209.98$ K		
1001.4	160.996	71
932.4	162.002	59
867.6	162.936	57
789.7	164.032	44
722.5	164.963	43
650.2	165.948	35
575.4	166.949	38
508.3	167.833	43
477.4	168.235	46
416.2	169.035	56
367.7	169.645	68
241.0	171.240	66
240.9	171.239	68
157.8	172.264	74
103.8	172.920	106
$T = 220.05$ K		
1001.9	166.377	62
942.7	167.101	81
872.7	167.953	75
807.1	168.743	45
734.0	169.606	44
666.8	170.393	42
595.3	171.224	41
530.7	171.961	22
480.5	172.535	64
427.6	173.125	39
373.8	173.726	53
315.5	174.372	74
261.5	174.959	64
209.0	175.529	72
155.7	176.111	80
102.5	176.673	144
$T = 239.98$ K		
1008.2	175.845	63
925.2	176.600	52
863.2	177.159	55
805.1	177.681	47
711.9	178.513	45
640.6	179.144	31
584.2	179.642	43
506.3	180.322	63
348.8	181.697	108
299.4	182.114	117
251.6	182.521	78
201.0	182.954	91
151.7	183.372	88
102.1	183.804	95
$T = 260.00$ K		
1007.1	184.406	68
933.1	184.922	67
847.6	185.512	54
773.2	186.027	52
687.9	186.616	40
611.6	187.137	44
532.7	187.678	44
454.6	188.211	61
403.4	188.559	67
350.7	188.918	59
304.8	189.229	68
249.3	189.605	71
201.6	189.928	84
148.7	190.293	89
100.4	190.623	90
$T = 280.00$ K		
985.8	192.350	60
925.8	192.675	54
869.4	192.979	53
799.3	193.360	42
734.5	193.706	44
660.7	194.109	37
593.8	194.465	53
533.8	194.791	52
479.7	195.084	54
421.8	195.399	70
362.9	195.718	69
298.9	196.066	80
240.9	196.379	77
181.8	196.700	84
123.1	197.025	72
65.7	197.351	95
$T = 300.00$ K		
1006.0	199.547	55
940.3	199.826	45
898.8	200.002	43
802.8	200.410	38
716.9	200.777	35
654.7	201.043	37
584.3	201.346	41
509.6	201.666	43
454.7	201.902	49
396.5	202.153	53
345.6	202.373	60
287.7	202.625	65
239.6	202.835	67
185.6	203.072	79
114.7	203.388	73
75.5	203.577	49
$T = 320.00$ K		
1524.0	204.757	46
1436.7	205.030	48
1334.1	205.363	49
1333.2	205.363	49
1241.7	205.665	41
1156.2	205.945	35

Table I. *(Continued)*

p (kPa)	u ($m \cdot s^{-1}$)	$10^6 \frac{\sigma[u]}{u}$	p (kPa)	u ($m \cdot s^{-1}$)	$10^6 \frac{\sigma[u]}{u}$	p (kPa)	u ($m \cdot s^{-1}$)	$10^6 \frac{\sigma[u]}{u}$
1051.4	206.291	37	1246.3	218.842	21	1488.9	230.757	98
956.0	206.607	42	1150.1	219.030	17	1360.5	230.888	86
848.7	206.967	48	1061.7	219.205	5	1281.4	230.970	75
753.2	207.288	55	954.0	219.420	6	1171.8	231.086	65
652.2	207.628	68	857.3	219.616	17	1042.1	231.227	50
606.9	207.782	70	749.9	219.835	30	955.0	231.323	45
551.3	207.971	74	656.1	220.030	38	851.7	231.442	36
488.8	208.184	84	558.6	220.233	50	738.9	231.571	28
433.2	208.375	85	502.0	220.354	56	631.2	231.698	21
384.1	208.543	91	450.8	220.462	61	549.6	231.796	20
324.2	208.749	103	405.0	220.561	66	508.3	231.847	22
267.2	208.949	103	354.3	220.671	70	448.2	231.922	30
215.0	209.132	111	301.8	220.786	73	406.7	231.975	39
156.7	209.337	119	278.4	220.838	74	354.4	232.040	40
101.4	209.540	101	201.8	221.008	79	302.9	232.105	43
			150.3	221.125	76	250.9	232.174	44
	$T = 340.00$ K		100.7	221.242	73	220.3	232.218	67
1508.3	211.740	40				213.9	232.227	59
1429.3	211.937	38		$T = 380.00$ K		99.2	232.379	96
1324.9	212.199	26	1557.1	224.597	62			
1228.4	212.443	17	1513.4	224.658	56			
1167.9	212.598	9	1390.3	224.833	44		$T = 425.00$ K	
1056.0	212.885	4	1313.7	224.943	35	1596.9	238.055	79
979.1	213.084	10	1206.9	225.098	25	1498.1	238.109	89
885.2	213.330	18	1108.8	225.243	20	1405.6	238.165	81
800.1	213.553	30	1018.7	225.379	11	1278.1	238.243	68
705.2	213.805	39	909.9	225.544	12	1199.5	238.294	62
605.7	214.070	48	812.8	225.694	25	1090.8	238.365	51
547.4	214.227	57	706.0	225.862	33	961.6	238.454	39
494.7	214.369	61	596.3	226.036	48	874.9	238.516	30
435.7	214.530	67	548.0	226.115	48	747.8	238.607	20
383.6	214.672	72	503.7	226.187	56	659.7	238.673	11
321.2	214.845	79	450.2	226.274	68	547.0	238.760	15
268.7	214.990	83	402.4	226.353	71	498.2	238.801	22
213.8	215.145	84	349.8	226.442	79	453.7	238.837	26
157.4	215.305	85	304.0	226.519	78	400.7	238.882	31
102.3	215.465	87	249.8	226.612	81	353.9	238.921	38
			199.8	226.701	85	303.1	238.966	41
	$T = 360.00$ K		151.3	226.791	139	259.7	239.005	42
1553.7	218.252	26	100.0	226.869	123	203.1	239.057	48
1545.0	218.270	26				149.6	239.111	60
1463.6	218.424	36		$T = 400.00$ K		117.3	239.144	57
1350.4	218.641	26	1581.3	230.667	61	100.9	239.163	60

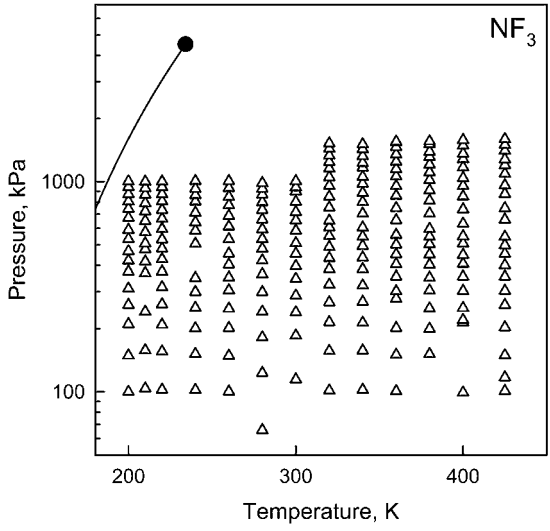

Fig. 1. Nitrogen trifluoride phase diagram. The individual states where $u(T, p)$ was measured are indicated by △. Also shown are the vapor pressure curve [4, 5] and the critical point at $T_c = 510$ K [3] and $p_c = 4.4$ MPa [5].

relative standard deviation $\sigma[u]/u \times 10^6$ with coverage factor of $k = 1$ are also listed in Table I.

3.2. Ethylene Oxide, C_2H_4O

Ethylene oxide is the precursor of polyethylene oxide which is used throughout semiconductor manufacturing. The purity of the sample studied here was 99.96%, by volume. The manufacturer only certified this composition for three months, because polymerization will occur during storage at room temperature. Our measurements showed evidence of this polymerization. To fill the resonator with ethylene oxide vapor at pressures above the vapor pressure at ambient temperature (approximately 100 kPa, Fig. 2), we first attempted to follow our customary procedure. A portion of the sample was placed in a small volume which was then heated along with the gas manifold. When the heated gas was admitted into the resonator, we found that the speed of sound in the gas was anomalously high, presumably as a result of the hydrogen liberated when the ethylene oxide polymerized. This problem forced us to use another technique. First, a series of low pressure isotherms were measured with the maximum pressure limited to the room temperature vapor pressure. Then, higher pressures were then

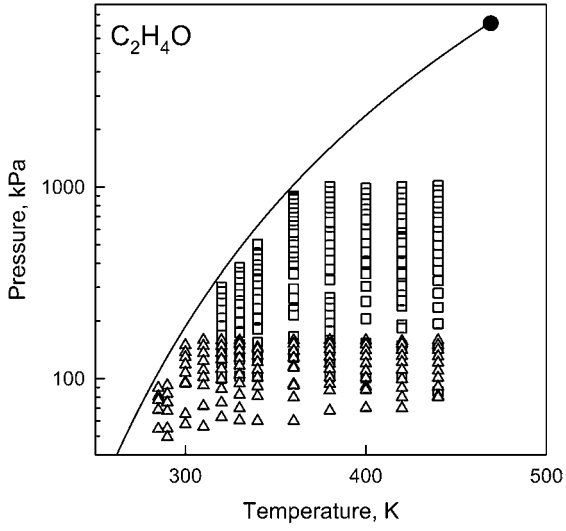

Fig. 2. Ethylene oxide phase diagram. The individual states where $u(T, p)$ was measured are indicated by △ for the low pressure isotherms and □ for the high pressure isotherms. The vapor pressure [8, 9] and critical point are shown, where $T_c = 469.15$ and $p_c = 7.19$ MPa [10].

achieved by transferring a portion of liquid ethylene oxide into the resonator by gently heating the sample and manifold. The resonator was then isolated and the temperature increased to the desired isotherm. Small portions of the sample were removed until the pressure was reduced to 80% of the sample's vapor pressure. Usually, this technique led to reproducible results and the high pressure data smoothly joined the lower pressure data within experimental uncertainties. On occasion, even this technique failed as indicated by the failure of the high pressure isotherm to smoothly join the corresponding low pressure data. When this occurred, the data were discarded, the apparatus was flushed, and a fresh aliquot of liquid sample was loaded.

An additional test was performed to look for possible polymerization of the C_2H_4O in the resonator at 380 and 440 K. A sample at 100 kPa was maintained in the resonator for 6 hours, the approximate time required to complete measurements along an isotherm. The resonance frequencies were repeatedly measured. The results showed that the resonance frequencies remained constant within experimental uncertainties. This test verified that once the sample was loaded into the resonator, the composition remained constant during the period of time required to make the measurements along a isotherm.

Figure 2 shows each state where the speed of sound was measured, with differing symbols for the low and high pressure data. Also shown are the vapor pressure curve [8, 9] and the critical point. The critical parameters have been reported as $T_c = 469.15$, $P_c = 7.19$ MPa, and $\rho_c = 7.1278$ kmol·m^{-3} [10]. The triple point temperature of ethylene oxide is approximately 160.65 K [11]. The speed of sound in ethylene oxide is listed in Tables IIa and IIb at 338 state points along 12 isotherms between 285 and 440 K. Higher pressure data are reported at or above 320 K in Table IIb. At each temperature and pressure, two longitudinal and one radial modes were used to compute the tabulated values of the speed of sound. The weighted mean of these three values and their relative standard deviation $\sigma[u]/u \times 10^6$ with a coverage factor of $k = 1$ are listed.

3.3. Trimethyl Gallium, $Ga(CH_3)_3$

Trimethyl gallium is used primarily for epitaxial metal-organic chemical vapor deposition (MOCVD), which requires a very high purity material (99.999 to 99.9999% mass fraction). The sample studied was five nines or better by weight. Trimethyl gallium is pyrophoric and has a normal boiling point of 328.95 K [12]. This limited the temperature range where measurements could be performed. The same loading technique that was used for ethylene oxide was employed here. Liquid trimethyl gallium was transferred to the resonator at room temperature by gently heating the source bottle and manifold. The resonator was then isolated and the temperature increased to the desired set point. Once the temperature stabilized, portions of the sample were removed until the pressure was at or below 80% of the vapor pressure. The speed of sound was measured at 218 states along 7 isotherms between 350 and 420 K. Figure 3 shows each state where the speed of sound was measured. Also shown are the vapor pressure curve [12, 13] and an estimate of the critical point. The average ratio of the critical temperature to the normal boiling point temperature for organic/inorganic compounds and inorganic halide compounds is 1.55. This ratio and the normal boiling point of 328.95 K [12] leads to the estimate of $T_c \approx 510$ K. The critical pressure $P_c \approx 4.4$ MPa was estimated by extrapolating the vapor pressure curve to the estimated critical temperature.

The measured speeds of sound in trimethyl gallium are reported in Table III. At each temperature and pressure, two longitudinal and one radial modes were used to compute the tabulated values of the speed of sound. The weighted mean of these three values and their relative standard deviation $\sigma[u]/u \times 10^6$ with a coverage factor of $k = 1$ are also listed.

Table IIa. Measured Speeds of Sound in Ethylene Oxide at Low Pressures

p (kPa)	u ($m \cdot s^{-1}$)	$10^6 \frac{\sigma[u]}{u}$
	$T = 285.00$ K	
89.5	251.703	170
89.5	251.704	173
80.7	252.212	116
77.2	252.402	114
68.7	252.866	96
54.6	253.610	54
	$T = 290.00$K	
92.4	253.706	99
92.3	253.706	97
83.3	254.168	89
75.1	254.581	81
67.7	254.952	86
54.9	255.573	53
49.5	255.844	79
	$T = 300.00$K	
149.8	255.175	170
137.5	255.762	103
129.6	256.128	93
118.6	256.631	85
107.2	257.145	80
95.8	257.655	77
94.3	257.721	77
65.3	258.998	73
57.7	259.323	71
	$T = 310.00$K	
159.5	259.013	87
148.2	259.476	84
136.3	259.962	78
123.8	260.466	76
111.0	260.982	73
101.8	261.348	67
92.2	261.730	75
71.9	262.523	54
56.1	263.149	51
	$T = 320.00$ K	
158.9	263.118	85
159.5	263.118	85
148.3	263.509	85
136.4	263.943	85
126.0	264.321	75
112.5	264.811	78
99.3	265.284	78
88.2	265.679	81
74.9	266.158	77
62.8	266.584	55
	$T = 330.00$ K	
158.3	267.085	68
152.0	267.294	68
140.8	267.666	68
128.2	268.080	64
117.0	268.449	66
105.0	268.842	62
94.4	269.186	56
82.4	269.577	59
70.0	269.975	46
60.4	270.279	39
	$T = 340.00$ K	
145.7	271.310	73
142.8	271.399	72
131.9	271.724	73
122.2	272.014	72
111.3	272.342	73
101.5	272.633	68
91.1	272.940	70
80.9	273.242	76
60.1	273.849	80
60.1	273.850	59
	$T = 360.00$ K	
158.7	278.253	67
158.7	278.253	66
158.7	278.254	69
151.8	278.431	69
139.5	278.744	66
128.5	279.022	67
116.2	279.331	64
113.9	279.391	67
93.8	279.894	60
92.1	279.940	59
79.6	280.251	64
60.0	280.746	91
60.0	280.749	79
	$T = 380.00$ K	
159.0	285.328	62
151.8	285.483	63
142.1	285.693	63
130.4	285.947	54
119.8	286.176	62
112.5	286.332	63
101.6	286.572	67
93.8	286.743	68
86.6	286.894	80
68.0	287.295	65
68.0	287.289	77
	$T = 400.00$ K	
89.5	292.185	66
158.7	292.187	65
150.9	292.330	69
140.7	292.526	67
131.3	292.700	60
120.0	292.912	60
109.9	293.101	56
100.9	293.272	56
90.9	293.459	64
87.3	293.529	74
70.3	293.844	75
	$T = 420.00$ K	
157.1	298.866	61
156.9	298.874	64
156.6	298.878	63
152.3	298.955	71
141.2	299.132	61
131.3	299.297	62
122.2	299.446	65
111.3	299.627	59
99.4	299.818	59
89.4	299.993	69
80.0	300.146	70
70.1	300.317	84
70.0	300.321	63
	$T = 440.00$ K	
158.7	305.345	53
149.7	305.482	56
141.5	305.600	53
130.9	305.756	50
121.2	305.899	55
110.1	306.060	50
101.0	306.197	60
90.7	306.344	64
81.0	306.495	82
79.9	306.511	77

Table IIb. Measured Speeds of Sound in Ethylene Oxide at Higher Pressures

p (kPa)	u ($m \cdot s^{-1}$)	$10^6 \frac{\sigma[u]}{u}$
	$T = 320.00$ K	
89.5	260.482	112
217.1	260.903	109
197.4	261.668	113
179.4	262.350	120
160.5	263.061	119
139.3	263.854	126
120.9	264.529	127
99.9	265.294	124
	$T = 320.00$ K	
301.3	257.596	67
284.9	258.237	96
263.8	259.089	121
248.6	259.685	77
228.5	260.476	107
207.3	261.296	105
188.6	262.012	125
168.9	262.758	140
148.9	263.506	141
127.3	264.304	139
102.4	265.219	149
	$T = 320.00$ K	
301.3	257.555	156
284.9	258.196	146
263.8	259.048	114
248.6	259.645	121
228.5	260.435	94
207.3	261.256	89
188.6	261.971	58
168.9	262.717	46
148.9	263.465	39
127.3	264.262	34
102.4	265.177	18
102.4	265.171	33
	$T = 330.00$ K	
379.9	259.259	193
380.0	259.252	183
379.9	259.262	193
359.2	259.996	341
342.1	260.643	191
318.7	261.518	50
296.5	262.313	46
275.3	263.065	30
255.2	263.748	160
244.4	264.130	88
221.9	264.911	81
197.0	265.775	6
173.7	266.558	29
150.5	267.327	68
126.2	268.131	76
102.9	268.901	62
102.9	268.898	67
	$T = 340.00$ K	
503.7	259.676	256
453.3	261.410	110
442.6	261.774	107
420.1	262.538	108
420.2	262.536	104
391.3	263.502	93
371.4	264.163	82
348.8	264.904	79
331.9	265.453	75
329.9	265.518	71
327.9	265.576	76
306.0	266.289	72
280.2	267.112	66
259.0	267.783	61
232.6	268.611	65
205.9	269.442	62
181.2	270.200	64
154.5	271.012	63
127.7	271.822	57
102.3	272.580	57
	$T = 360.00$ K	
896.1	257.227	56
876.3	257.873	60
864.1	258.268	66
819.9	259.669	61
819.9	259.668	61
774.6	261.081	70
774.6	261.080	69
734.3	262.317	73
734.3	262.313	65
696.2	263.469	75
696.2	263.468	73
660.8	264.527	84
627.8	265.500	75
597.2	266.392	73
569.2	267.199	70
519.4	268.621	75
497.6	269.235	72
460.5	270.271	78
430.2	271.111	79
406.0	271.772	79
386.7	272.297	78
357.8	273.078	81
351.5	273.246	81
295.0	274.756	84
262.6	275.608	87
229.9	276.461	88
214.9	276.850	86
166.1	278.106	90
134.8	278.899	92
133.6	278.926	90
132.5	278.953	90
131.4	278.980	86
130.3	279.007	89
129.2	279.036	88
	$T = 380.00$ K	
265.7	283.016	55
249.3	283.365	108
233.6	283.724	50
214.9	284.134	53
194.9	284.573	45
177.2	284.954	57
158.8	285.357	63

Table IIb. *(Continued)*

p (kPa)	u ($m \cdot s^{-1}$)	$10^6 \frac{\sigma[u]}{u}$	p (kPa)	u ($m \cdot s^{-1}$)	$10^6 \frac{\sigma[u]}{u}$	p (kPa)	u ($m \cdot s^{-1}$)	$10^6 \frac{\sigma[u]}{u}$
139.9	285.765	57	602.1	283.568	17	827.0	287.532	45
121.5	286.162	54	567.9	284.256	14	771.8	288.511	39
102.1	286.571	66	508.0	285.456	16	770.4	288.541	46
102.1	286.577	58	507.6	285.462	13	720.2	289.418	39
102.1	286.584	64	507.1	285.467	35	630.5	290.985	43
102.1	286.577	50	458.6	286.435	19	589.6	291.694	60
102.1	286.587	77	402.4	287.539	22	552.5	292.341	36
102.1	286.580	65	353.2	288.495	23	487.8	293.440	27
102.1	286.583	47	303.4	289.455	31	459.6	293.923	37
102.0	286.597	110	253.3	290.418	13	410.9	294.768	35
102.0	286.574	71	205.6	291.334	25	371.5	295.414	31
102.0	286.581	65	153.5	292.304	23	325.9	296.164	21
102.0	286.582	55	100.9	293.291	29	285.2	296.847	33
						239.3	297.617	67
	$T = 380.00$ K			$T = 420.00$ K		191.2	298.402	21
1008.7	265.038	53				148.7	299.107	53
949.6	266.583	92	1008.5	284.225	58	102.6	299.859	71
891.7	268.087	47	941.2	285.461	48			
837.5	269.473	65	939.4	285.486	42		$T = 440.00$ K	
787.2	270.742	83	878.7	286.559	46	1019.2	292.541	80
740.5	271.903	88	821.6	287.604	45	962.1	293.435	85
696.8	272.979	83	768.7	288.537	39	908.2	294.270	91
656.3	273.962	50	689.4	289.938	46	841.9	295.293	86
584.4	275.692	83	687.9	289.966	39	789.4	296.096	86
552.9	276.431	63	645.5	290.717	43	741.2	296.832	96
497.0	277.745	96	539.7	292.531	60	696.3	297.512	95
451.0	278.820	42	510.1	293.044	36	656.0	298.115	99
414.2	279.663	33	461.1	293.892	27	585.7	299.168	90
372.2	280.622	44	403.5	294.844	37	553.2	299.650	100
327.8	281.620	67	352.1	295.693	35	495.2	300.516	98
			305.5	296.503	31	444.8	301.254	112
	$T = 400.00$ K		255.7	297.313	21	402.9	301.895	100
988.2	275.478	14	183.7	298.453	33	366.9	302.401	95
928.7	276.765	6				324.6	303.019	90
871.6	277.984	7		$T = 420.00$ K		279.6	303.667	93
817.4	279.130	2	1008.7	284.2471	58	235.6	304.303	87
767.1	280.182	3	992.2	284.551	48	193.5	304.920	94
721.0	281.140	7	928.1	285.714	42	143.0	305.629	90
677.7	282.030	15	885.5	286.477	46	85.4	306.447	89

Table III. Measured Speeds of Sound in Trimethyl Gallium

p (kPa)	u ($m \cdot s^{-1}$)	$10^6 \frac{\sigma[u]}{u}$	p (kPa)	u ($m \cdot s^{-1}$)	$10^6 \frac{\sigma[u]}{u}$	p (kPa)	u ($m \cdot s^{-1}$)	$10^6 \frac{\sigma[u]}{u}$
$T = 340.00$ K			72.1	164.223	77	40.7	167.870	80
			61.2	164.690	93	40.7	167.871	59
89.5	156.503	154	51.4	165.100	101	40.7	167.869	35
111.8	156.998	106	41.2	165.523	104	40.6	167.872	49
101.8	157.548	86	30.6	165.961	120	40.7	167.877	40
90.0	158.185	71	30.6	165.974	174	40.6	167.875	64
81.6	158.623	70	30.6	165.977	191	40.7	167.876	49
70.6	159.196	65	30.7	165.967	152			
60.8	159.695	64	30.6	165.982	199	$T = 380.00$ K		
51.5	160.165	66	30.6	165.980	196			
40.3	160.726	71	30.6	165.984	177	320.5	159.482	50
30.1	161.238	92	30.6	165.983	191	305.2	160.118	53
			30.6	165.977	145	276.5	161.295	53
$T = 350.00$ K			30.6	165.975	154	263.4	161.827	57
			30.5	165.981	147	239.3	162.789	55
161.4	157.363	109	30.6	165.976	162	217.1	163.657	53
155.3	157.689	102				196.7	164.440	56
143.1	158.306	85				178.4	165.143	52
130.9	158.927	82	$T = 370.00$ K			161.6	165.778	52
124.0	159.264	70				139.2	166.608	58
112.2	159.834	66	291.2	157.444	82	139.2	166.610	47
101.7	160.339	63	282.9	157.831	74	132.5	166.854	54
92.0	160.801	60	274.7	158.204	60	120.5	167.298	54
81.2	161.306	58	260.7	158.842	66	109.6	167.695	71
71.4	161.766	59	247.1	159.449	54	99.3	168.067	58
61.0	162.245	62	239.9	159.763	55	90.2	168.396	54
51.4	162.689	51	227.3	160.312	51	78.0	168.835	64
40.7	163.181	42	215.4	160.831	47	70.7	169.088	71
31.0	163.619	65	204.0	161.317	51	60.9	169.434	70
			193.1	161.777	47	50.3	169.817	52
$T = 360.00$ K			178.9	162.374	53	50.3	169.818	55
			169.5	162.768	50	50.3	169.820	82
220.3	157.505	56	157.0	163.276	50	50.4	169.818	55
209.4	158.039	47	145.7	163.741	50	50.3	169.820	55
198.2	158.582	24	134.8	164.182	46	50.3	169.817	91
187.4	159.095	26	121.5	164.717	50	50.3	169.817	70
177.2	159.573	29	112.1	165.093	47	50.3	169.809	82
163.3	160.207	37	100.7	165.541	54	50.3	169.818	62
154.4	160.615	40	92.7	165.856	53	50.1	169.823	94
142.7	161.141	44	81.4	166.299	55	50.3	169.817	16
133.1	161.570	46	71.1	166.699	53	50.3	169.820	134
121.4	162.090	51	60.4	167.107	61	50.4	169.825	80
113.0	162.457	54	51.5	167.455	59	50.3	169.819	65
101.7	162.954	58	40.5	167.872	36	50.3	169.827	112
91.6	163.386	66	40.6	167.869	33			
82.2	163.790	70						

Table III. *(Continued)*

p (kPa)	u ($m \cdot s^{-1}$)	$10^6 \frac{\sigma[u]}{u}$	p (kPa)	u ($m \cdot s^{-1}$)	$10^6 \frac{\sigma[u]}{u}$
50.3	169.825	107	40.9	174.557	58
50.3	169.821	64	40.9	174.555	67
50.3	169.819	85			
50.3	169.826	98		$T = 420.00$ K	
			158.7	152.528	58
	$T = 400.00$ K		849.5	153.941	74
597.3	155.241	43	812.3	155.340	77
582.0	155.870	33	812.4	155.341	82
566.8	156.485	20	776.1	156.665	83
539.8	157.565	19	740.7	157.939	88
513.6	158.588	23	715.0	158.837	82
499.6	159.133	23	682.3	159.972	83
474.6	160.082	27	682.4	159.973	80
450.2	160.991	30	650.1	161.066	79
426.7	161.856	31	619.2	162.094	68
404.1	162.681	35	588.8	163.087	65
391.6	163.127	34	560.3	164.010	61
360.7	164.223	32	560.3	164.010	66
331.2	165.247	44	533.1	164.873	62
303.5	166.199	48	507.5	165.679	64
277.2	167.080	48	483.4	166.424	62
253.1	167.887	53	438.9	167.787	61
224.4	168.825	50	418.8	168.392	67
198.6	169.662	54	399.4	168.970	65
168.9	170.606	56	370.6	169.821	61
143.1	171.415	57	345.3	170.558	60
129.2	171.852	60	324.1	171.172	60
120.6	172.108	56	296.8	171.951	59
113.2	172.347	58	280.5	172.413	57
101.9	172.695	56	269.2	172.733	49
91.6	173.009	59	261.1	172.961	55
82.3	173.292	58	254.4	173.147	50
71.9	173.611	52	249.7	173.281	54
60.1	173.964	62	246.0	173.383	52
52.4	174.199	63	242.4	173.486	52
40.9	174.546	70	239.2	173.572	54
40.9	174.545	58	236.4	173.652	53
40.9	174.548	65	233.8	173.727	54
40.9	174.551	60	231.3	173.794	54
40.9	174.554	83	228.3	173.877	53
40.9	174.549	55	225.1	173.965	53
40.9	174.548	52	224.0	173.996	56

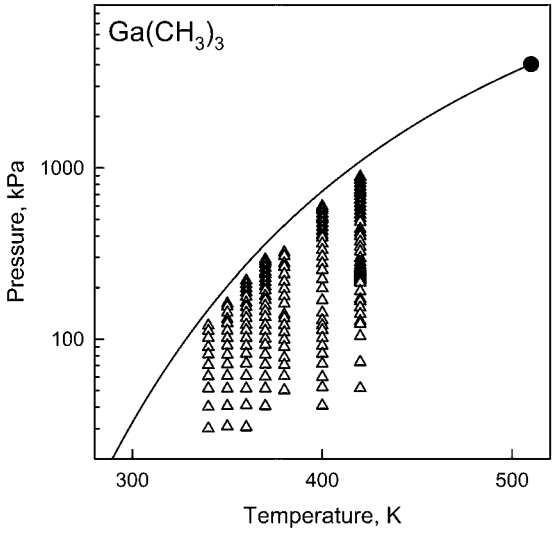

Fig. 3. Trimethyl gallium phase diagram. The individual states where $u(T, p)$ was measured are indicated by △. Also shown is the vapor pressure [12, 13] and the critical point estimated at $T_c \approx 510$ K and $p_c \approx 4.4$ MPa.

4. ACOUSTIC EQUATION OF STATE

The speed-of-sound data were collected along isotherms. The data on each isotherm were fitted by the acoustic virial equation of state:

$$u^2 = \frac{\gamma^0 RT}{m}\left(1+\frac{\beta_a p}{RT}+\frac{\gamma_a p^2}{RT}+\frac{\delta_a p^3}{RT}+\cdots\right) \tag{1}$$

where m is the molar mass, R is the universal gas constant, T is the temperature in kelvin (ITS-90), C_p^0 is the constant-pressure ideal-gas heat capacity, $\gamma^0 = C_p^0/C_v^0$ is the zero-pressure limit of the heat-capacity ratio, and β_a, γ_a, and δ_a are the temperature-dependent acoustic virial coefficients. On each isotherm, C_p^0 was obtained from the zero-pressure intercept of Eq. (1) through the relation $C_p^0/R = \gamma^0/(\gamma^0 - 1)$. The heat capacities were fitted by a polynomial function in temperature:

$$C_p^0(T)/R = A_0 + A_1 T + A_2 T^2 + A_3 T^3 \tag{2}$$

Table IV. Nitrogen Trifluoride

T (K)	C_p^0 (R)	β_a ($cm^3 \cdot mol^{-1}$)	γ_a ($cm^3 \cdot mol^{-1} \cdot MPa^{-1}$)
199.98	5.1519 ± 0.0043	−258.45 ± 0.84	−26.61 ± 0.91
209.98	5.2855 ± 0.0033	−235.25 ± 0.53	−17.97 ± 0.47
220.05	5.4217 ± 0.0031	−215.00 ± 0.49	−11.22 ± 0.43
239.98	5.6872 ± 0.0038	−181.15 ± 0.64	−3.15 ± 0.57
260.00	5.9528 ± 0.0037	−152.41 ± 0.58	0.62 ± 0.52
280.00	6.2074 ± 0.0038	−129.04 ± 0.58	3.09 ± 0.53
300.00	6.4551 ± 0.0041	−107.98 ± 0.59	3.53 ± 0.51
320.00	6.6938 ± 0.0041	−89.81 ± 0.43	3.55 ± 0.26
340.00	6.9137 ± 0.0033	−74.56 ± 0.35	3.73 ± 0.21
360.00	7.1211 ± 0.0033	−60.99 ± 0.34	3.59 ± 0.20
380.00	7.3108 ± 0.0051	−49.13 ± 0.44	3.61 ± 0.25
400.00	7.4887 ± 0.0041	−39.02 ± 0.41	3.69 ± 0.24
425.00	7.6726 ± 0.0034	−28.24 ± 0.37	3.97 ± 0.22

4.1. Nitrogen Trifluoride, NF_3

The nitrogen trifluoride was well behaved; there was no evidence of decomposition. Its low normal boiling point, 66.5 K, allowed measurements at 1 MPa or higher over the entire temperature range. The ideal-gas heat capacities and acoustic virial coefficients obtained from fitting Eq. (1) to each isotherm are given in Table IV. The standard uncertainties for the heat capacities are all less than 0.1% as expected from prior experience with this apparatus. Equation (2) was fit to the data in Table IV, and the resulting parameters are listed in Table V. Figure 4 shows the deviations of the tabulated heat capacities from Eq. (2). Also shown are values determined from spectroscopy and statistical mechanics. The agreement is reasonable because the spectroscopically-determined values have uncertainties on the order of 1%.

Table V. Parameters for Calculated $C_p^0(T)/R$ from Eq. (2)

	Nitrogen trifluoride	Ethylene oxide	Trimethyl gallium
A_0	2.71143	5.50623	183.17152
A_1 (K^{-1})	9.16575×10^{-3}	-2.47935×10^{-2}	−1.39258
A_2 (K^{-2})	2.33790×10^{-5}	1.18723×10^{-4}	3.75667×10^{-3}
A_3 (K^{-3})	-4.11288×10^{-8}	-1.10791×10^{-7}	-3.29944×10^{-6}

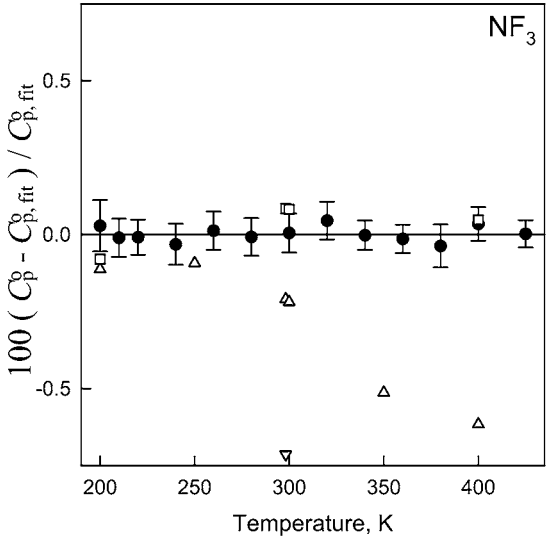

Fig. 4. Deviations of C_p^0 from Eq. (2) for NF_3. (●) Present work; (△) [29]; (□) [30]; (□) [31].

4.2. Ethylene Oxide, C_2H_4O

As discussed in Section 3.2 the low-pressure and high-pressure data for ethylene oxide were obtained in separate runs. The low pressure data were used to determine C_p^0 and the acoustic virial coefficients reported in Table VI. The limited pressure range resulted in increased uncertainties for

Table VI. Ethylene Oxide

T (K)	C_p^0 (R)	β_a ($cm^3 \cdot mol^{-1}$)	γ_a ($cm^3 \cdot mol^{-1} \cdot MPa^{-1}$)
285	5.567±0.10	−951±137	−1.70±0.94
290	5.598±0.05	−830±65	−0.63±0.46
300	5.763±0.01	−764±14	−0.38±0.07
310	5.929±0.02	−730±14	−0.16±0.06
320	6.099±0.02	−682±18	−0.10±0.08
330	6.277±0.02	−628±13	−0.10±0.06
340	6.439±0.01	−604.0±3.1	
360	6.797±0.01	−529.7±2.1	
380	7.152±0.01	−469.6±2.2	
400	7.495±0.01	−419.9±2.4	
420	7.825±0.01	−381.2±2.5	
440	8.145±0.01	−347.2±2.6	

the parameters in Eq. (1). The higher temperature isotherms (340 to 440 K) required only the first acoustic virial coefficient; the lower temperature isotherms (285 to 330 K) required also the second acoustic virial coefficient. The values of C_p^0 at the lower temperatures have even greater uncertainty because the fit included an additional fitting parameter for the same pressure range.

Figure 5 shows the deviations of the values of C_p^0 listed in Table VI from those calculated with Eq. (2) using the parameters listed in Table V. Figure 5 also shows published values of C_p^0 calculated from spectroscopy and statistical mechanics. Because the calculated values have uncertainties of 1% or more, the agreement is good.

4.3. Trimethyl Gallium, $Ga(CH_3)_3$

The relatively low vapor pressure of trimethyl gallium limited the ranges of temperature and pressure available for measuring $u(T, p)$. The values of C_p^0 determined by fitting Eq. (1) to each isotherm are reported in Table VII. Equation (2) was fitted to the data in Table VII and the resulting parameters provided in Table V. Figure 6 shows the deviations of the heat capacities in Table VII from Eq. (2). There is only one published value

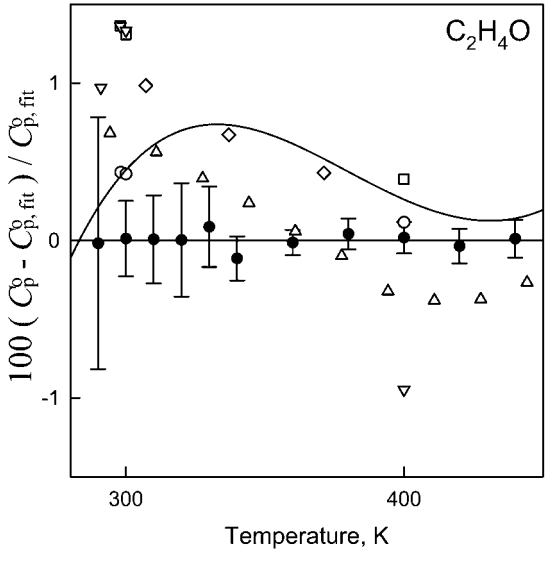

Fig. 5. Deviations of C_p^0 from Eq. (2) for C_2H_4O. (●) Present work; (——) [32]; (□) [33]; (△) [34]; (▽) [35]; (◇) [36]; (○) [37].

Table VII. Trimethyl Gallium

T (K)	C_p^0 (R)	β_a ($cm^3 \cdot mol^{-1}$)	γ_a ($cm^3 \cdot mol^{-1} \cdot MPa^{-1}$)
340	14.297 ± 0.10	-1663 ± 27	-0.620 ± 0.22
350	14.469 ± 0.05	-1552 ± 10	-0.414 ± 0.06
360	14.786 ± 0.04	-1440.2 ± 6.2	-0.378 ± 0.029
370	15.106 ± 0.03	-1337.9 ± 3.7	-0.314 ± 0.014
380	15.384 ± 0.03	-1251.1 ± 3.6	-0.262 ± 0.012
400	16.050 ± 0.04	-1108.2 ± 2.9	-0.166 ± 0.009
420	16.518 ± 0.03	-977.3 ± 1.1	-0.139 ± 0.001

of C_p^0 in this temperature range; it was calculated from spectroscopic data, and it agrees within 0.1% with our results.

5. VIRIAL EQUATION OF STATE

The virial equation of state is

$$p = RT\rho[1 + B(T)\,\rho + C(T)\,\rho^2 + \cdots] \tag{3}$$

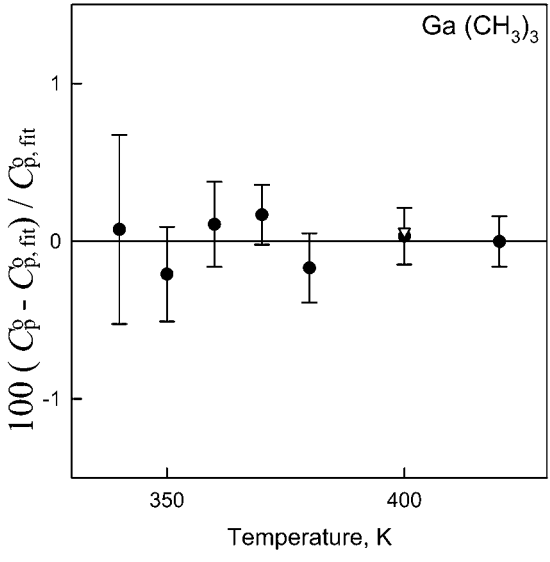

Fig. 6. Deviations of C_p^0 from Eq. (2) for $Ga(CH_3)_3$. (●) Present work; (△) [38].

where $B(T)$ and $C(T)$ are the second and third density virial coefficients. The acoustic virial coefficients in Eq. (1) are directly related to the density virial coefficients in Eq. (3) through exact thermodynamic relations involving the density virial coefficients, their temperature derivatives, and $\gamma^0(T)$ [14]. Equation (3) was fitted directly to the $u^2(T, p)$ surface for each of the three gases using these relationships together with a model for the temperature dependence of the density virial coefficients, and $\gamma^0(T)$ was computed from Eq. (2) and the parameters in Table V.

Two models for the density virial coefficients and their temperature dependence were considered: (1) the hard-core square-well (HCSW) model, and (2) the hard-core Lennard-Jones (HCLJ) model. The implementation of both of these models was described in detail elsewhere [1, 15–17]; here only the results are provided.

5.1. Hard-Core Square-Well Potential Model (HCSW)

The HCSW model is an algebraically simple representation of intermolecular interactions with the advantage of having explicit algebraic expressions for the temperature dependent second and third virial coefficients [14]. These expressions are

$$\begin{aligned} B(T) &= b_0[1-(\lambda^3-1)\,\Delta] \\ C(T) &= \tfrac{1}{8}b_0^2(5-c_1\Delta-c_2\Delta^2-c_3\Delta^3) \end{aligned} \tag{4}$$

$$\begin{aligned} c_1 &= \lambda^6-18\lambda^4+32\lambda^3-15 \\ c_2 &= 2\lambda^6-36\lambda^4+32\lambda^3+18\lambda^2-16 \\ c_3 &= 6\lambda^6-18\lambda^4+18\lambda^2-6 \end{aligned} \tag{5}$$

where $\Delta = \exp[\varepsilon/(k_B T)-1]$ and k_B is Boltzmann's constant. The adjustable parameters are as follows: ε is the well depth, σ is the hard-core diameter, and λ is the ratio of the width of the well to σ. Here b_0 is the molar volume of the hard core $b_0 = \frac{2}{3}\pi N_A \sigma^3$, and N_A is Avogadro's constant. Equations (4) and (5) allow a $u^2(T, p)$ surface to be fitted directly to Eq. (3). As in Ref. 14, different values of b_0, ε, and λ were used for $B(T)$ and $C(T)$. This resulted in a model having six adjustable parameters. Equations (4) and (5) provide reasonable temperature dependences for $B(T)$ and $C(T)$; however, the magnitudes of the fitted parameters have no physical significance. The six parameters [b_0, ε, and λ for $B(T)$ and b_0, ε, and λ for $C(T)$] in Eqs. (4) and (5) were fitted to the $u^2(T, p)$ surface for each gas, while C_p^0 was fixed at the values given by Eq. (2) with the parameters in Table V.

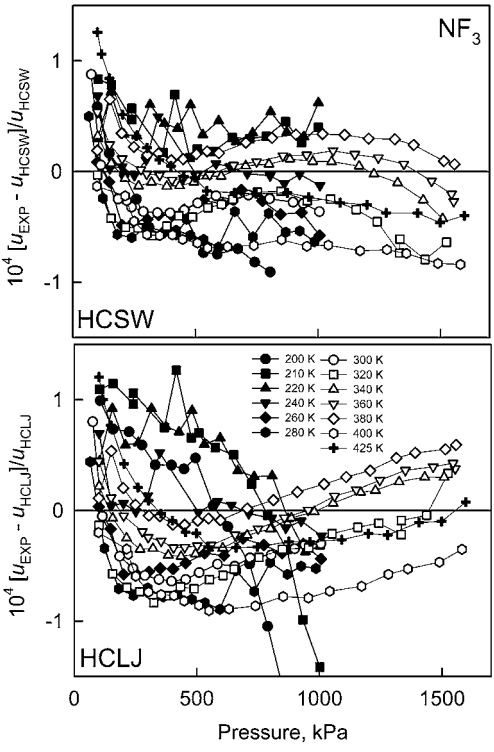

Fig. 7. Deviation plot of measured speeds of sound in NF_3 from the fitted virial equations of state.

5.1.1. Nitrogen Trifluoride, NF_3

Equation (3) was fitted to the $u^2(T, p)$ surface for nitrogen trifluoride using the HCSW model. The resulting parameters are listed in Table VIII. The fit had 223 degrees of freedom, v, and χ^2/v was 0.89, where $\chi^2 = \sum_i [f(x_i) - f_i]^2/\sigma_f^2$; and $f(x_i) = u^2(T, p)$. Figure 7 (top) shows the deviation plot of the measured speeds of sound from the HCSW equation of state. Nearly all the data are reproduced by the equation of state to within $\pm 0.01\%$. There are small systematic positive deviations at the lowest pressures, which might be caused by errors in the estimated transport properties used to reduce the speed-of-sound data.

5.1.2. Ethylene Oxide, C_2H_4O

The ethylene oxide data set included the low-pressure and high-pressure isotherms. The high-pressure isotherms at 320, 380, and 420 K were

Table VIII. HCSW Parameters

	$B(T)$ $(m^3 \cdot mol^{-1})$			$C(T)$ $(m^3 \cdot mol^{-1})^2$		
	b_0 $(m^3 \cdot mol^{-1})$	λ	ε/k_B (K)	b_0 $(m^3 \cdot mol^{-1})$	λ	ε/k_B (K)
NF_3	7.17029×10^{-5}	1.57265	167.709	6.90466×10^{-5}	1.90998	111.831
C_2H_4O	3.74429×10^{-5}	1.35607	769.986	2.65524×10^{-4}	1.08884	771.990
$Ga(CH_3)_3$	1.57924×10^{-5}	1.78755	919.390	3.35847×10^{-4}	1.15151	746.240

repeated to ensure reproducibility. Equation (3) was fitted to the entire $u^2(T, p)$ surface using the HCSW model. The resulting parameters are listed in Table VIII. The fit had 329 degrees of freedom, ν, and χ^2/ν was 2.47. Figure 8 (top) shows the deviation plot of the measured speeds of sound from the HCSW equation of state. Nearly all the measured speeds of

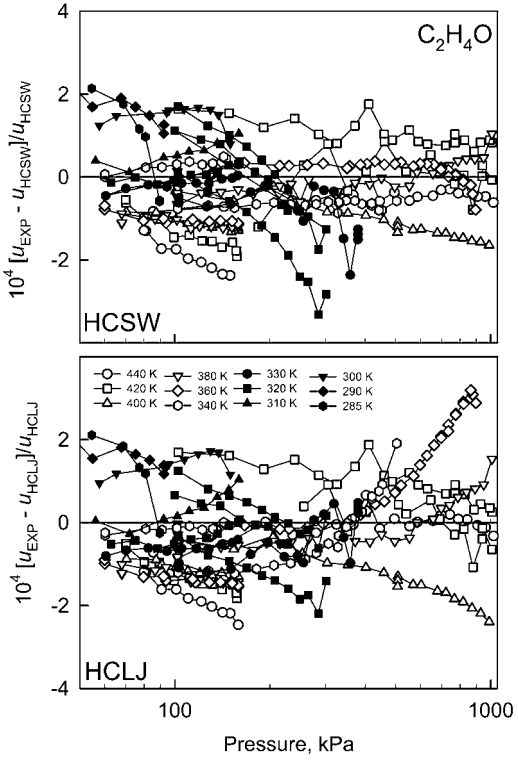

Fig. 8. Deviation plot of measured speeds of sound in C_2H_4O from the fitted virial equations of state.

sound are reproduced by the equation of state to better than 0.02%. In contrast with the NF_3 data, the deviations do not show a systematic pressure dependence at the lowest pressures at any temperature.

5.1.3. *Trimethyl Gallium, $Ga(CH_3)_3$*

As described above, the $u^2(T, p)$ data for trimethyl gallium were fitted by the HCSW model using Eq. (3). The 360, 370, and 380 K isotherms all had redundant measurements taken at the lowest pressure to ensure that no decomposition was occurring. The 360 K isotherm was repeated to insure reproducibility. The resulting parameters are listed in Table VIII. The fit had 208 degrees of freedom, ν, and χ^2/ν was 1.52. Figure 9 (top) shows the deviations of the measured speeds of sound from the HCSW equation of state. All of the speed-of-sound data are reproduced by the equation of state to within $\pm 0.02\%$.

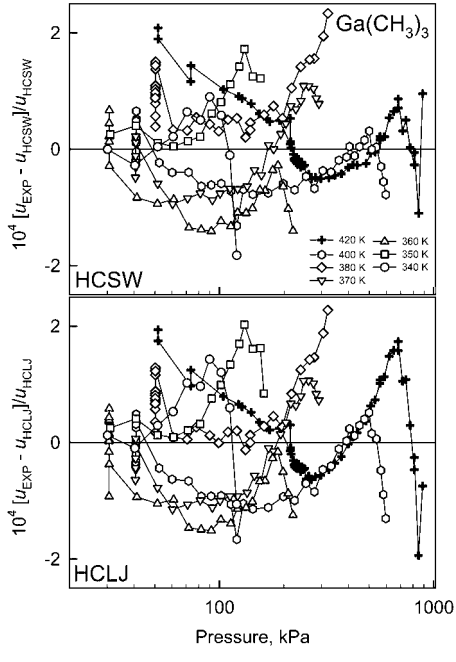

Fig. 9. Deviation plot of measured speeds of sound in $Ga(CH_3)_3$ from the fitted virial equations of state.

5.2. Hard-Core Lennard-Jones Model (HCLJ)

In this section, the square-well intermolecular potential is replaced by the more realistic hard-core Lennard-Jones 6-12 potential [18] given by,

$$\varphi(r_{ij}) = 4\varepsilon \left\{ \left(\frac{\sigma - 2a}{r_{ij} - 2a} \right)^{12} - \left(\frac{\sigma - 2a}{r_{ij} - 2a} \right)^{6} \right\} \tag{6}$$

where r_{ij} is the intermolecular separation between molecules i and j, ε is the well depth, σ is the value of r_{ij} where $\varphi(r)$ crosses zero, and a is the radius of the hard core. This potential has three adjustable parameters: ε, σ, and a. The HCLJ analysis is similar to that of the HCSW; however, multiple numerical integrations are required at each temperature to determine the virial coefficients and their temperature derivatives from Eq. (6). The classical second and third virial coefficients and their temperature derivatives [19, 20] were calculated using an automatic adaptive quadrature routine [21], where one can specify the desired accuracy, which was set to 10^{-4}. The calculation of the third virial coefficient required the inclusion of three-body contributions. Following Trusler [23], the Axilrod-Teller triple-dipole term [22] was included which added a fourth adjustable parameter, ν_{123} to the fit. This is the first term in the three-body corrections to the dispersion energy for monatomic species. The integral equations providing the second and third virial coefficients for spherically symmetric molecules are given in Ref. 23.

The HCLJ model is physically more accurate than the HCSW model. The potential approaches infinity as the intermolecular separation approaches zero, and the potential asymptotically approaches zero at large intermolecular separations. However, none of the molecules studied are either spherically symmetric or monatomic. Thus, the HCLJ (and the HCSW) potentials approximate spherical averages of the true potentials. Because the data are reproduced within their experimental uncertainties, we were not motivated to consider potentials that are anisotropic or that have a more complex shape than the HCLJ potential or more realistic approximations in the three-body corrections to the third virial coefficient.

With $C_p^0(T)$ given by Eq. (2) and the parameters in Table V, four potential parameters, ε, σ, a, and ν_{123} were used to fit the virial equation of state, Eq. (3), to the $u^2(T, p)$ surface for each gas. The more realistic HCLJ potential has two fewer parameters than the HCSW mode (Section 6.1), and it has more accurate virial coefficients upon extrapolation to high temperatures. Because the second and third virial coefficients are both calculated from the same model, the HCLJ potential is indeed a model of the intermolecular interactions.

Table IX. HCLJ Parameters

	σ (nm)	a (nm)	ε/k_B (K)	ν_{123}/k_B ($K \cdot nm^9$)
NF_3	0.40429	0.054396	276.96	0.006076
C_2H_4O	0.34580	0.076735	993.60	0.018037
$Ga(CH_3)_3$	0.30100	0.019143	1242.35	0.026652

5.2.1. Nitrogen Trifluoride, NF_3

Equation (3) was fitted to the $u^2(T, p)$ surface for nitrogen trifluoride using the HCLJ model. The resulting parameters are listed in Table IX. The fit had 225 degrees of freedom, ν, and χ^2/ν was 1.31. Figure 7 (bottom) shows the deviations of the measured speeds of sound from the HCLJ equation of state. The lowest temperature isotherms show greater deviations at higher pressures than seen in the HCSW model. Most likely, these deviations result from the neglect of a small contribution from the fourth virial $D(T)$ to $u^2(T, p)$. The HCSW model compensated for this neglect because it has two more adjustable parameters. Never the less, the resulting equation of state still nearly reproduces all the speed-of-sound data to within $\pm 0.01\%$.

5.2.2. Ethylene Oxide, C_2H_4O

As in the HCSW fit, the fit of the HCLJ mode to the ethylene oxide data included both the low and high-pressure isotherms. The resulting parameters are listed in Table IX. The fit had 332 degrees of freedom, ν, and χ^2/ν was 5.37. Figure 8 (bottom) shows the deviations of the measured speeds of sound from the HCLJ equation of state. Nearly all the measured speeds of sound are reproduced by the equation of state to within $\pm 0.02\%$.

5.2.3. Trimethyl Gallium, $Ga(CH_3)_3$

The trimethyl gallium speed of sounds were used to fit Eq. (3) using the HCLJ model as was done above. The resulting parameters are listed in Table IX. The fit had 217 degrees of freedom, ν, and χ^2/ν was 1.94. Figure 9 (bottom) shows the deviations of the measured speeds of sound from the HCLJ equation of state. Nearly all the measured speeds of sound are reproduced by the equation of state to within $\pm 0.02\%$.

5.3. Interpolation Tables

The computation of the second and third virial coefficients and their temperature derivatives for each of the three gases using the four potential

parameters found in Table IX is a numerically intensive process; thus, it is not practical for repetitive calculations. Look-up tables are provided for the second and third virial coefficients and their first two temperature derivatives for each of the three gases (Tables X–XII). These derivatives can be used to interpolate between listed values. In the look-up table, a substitution of variables has been performed. The temperature is replaced by a reduced reciprocal temperature $\tau = \varepsilon/k_B T$ where $T\frac{dB}{dT} = -\tau\frac{dB}{d\tau}$ and $T^2\frac{d^2B}{dT^2} = \tau^2\frac{d^2B}{d\tau^2} + 2\tau\frac{dB}{d\tau}$. Tables X–XII provides the virial coefficients in reduced

Table X. Nitrogen Trifluoride HCLJ Reduced Virial Coefficients, where $\tau = \varepsilon/k_B T$ and $\varepsilon/k_B = 276.96$ K and $B^*(T) = B(T)/(\frac{2}{3}\pi N_A\sigma^3)$ and $C^*(T) = C(T)/(\frac{2}{3}\pi N_A\sigma^3)^2$ where $\sigma = 0.40429$ nm

τ	$B(\tau)^*$	$\frac{\partial B(\tau)^*}{\partial\tau}$	$\frac{\partial^2 B(\tau)^*}{\partial\tau^2}$	$\frac{\partial^3 B(\tau)^*}{\partial\tau^3}$	$C(\tau)^*$	$\frac{\partial C(\tau)^*}{\partial\tau}$	$\frac{\partial^2 C(\tau)^*}{\partial\tau^2}$	$\frac{\partial^3 C(\tau)^*}{\partial\tau^3}$
0.2	0.050926	−0.144245	−0.312078	2.230609	0.003675	0.000376	−0.005324	0.274744
0.3	0.035208	−0.168188	−0.192694	0.589093	0.003720	0.000803	0.011006	0.095248
0.4	0.017501	−0.185375	−0.157540	0.189330	0.003869	0.002272	0.017522	0.043009
0.5	−0.001800	−0.200477	−0.146864	0.044797	0.004189	0.004190	0.020421	0.016855
0.6	−0.022578	−0.215070	−0.146112	−0.022472	0.004712	0.006282	0.021063	−0.003875
0.7	−0.044821	−0.229865	−0.150417	−0.060619	0.005444	0.008333	0.019591	−0.026174
0.8	−0.068571	−0.245256	−0.157828	−0.086253	0.006370	0.010118	0.015648	−0.053852
0.9	−0.093901	−0.261505	−0.167479	−0.106142	0.007450	0.011357	0.008536	−0.090077
1.0	−0.120907	−0.278813	−0.178971	−0.123416	0.008611	0.011686	−0.002765	−0.138264
1.1	−0.149705	−0.297354	−0.192130	−0.139685	0.009740	0.010618	−0.019651	−0.202528
1.2	−0.180425	−0.317293	−0.206905	−0.155859	0.010667	0.007508	−0.043978	−0.288057
1.3	−0.213215	−0.338790	−0.223318	−0.172508	0.011146	0.001494	−0.078191	−0.401495
1.4	−0.248240	−0.362013	−0.241436	−0.190025	0.010831	−0.008565	−0.125490	−0.551410
1.5	−0.285681	−0.387137	−0.261362	−0.208712	0.009248	−0.024178	−0.190054	−0.748871
1.6	−0.325738	−0.414350	−0.283226	−0.228821	0.005745	−0.047331	−0.277322	−1.008192
1.7	−0.368628	−0.443852	−0.307181	−0.250583	−0.000556	−0.080633	−0.394366	−1.347890
1.8	−0.414592	−0.475862	−0.333405	−0.274223	−0.010832	−0.127500	−0.550370	−1.791916
1.9	−0.463891	−0.510615	−0.362096	−0.299965	−0.026655	−0.192399	−0.757249	−2.371252
2.0	−0.516815	−0.548371	−0.393476	−0.328046	−0.050105	−0.281156	−1.030453	−3.125973
2.1	−0.573675	−0.589408	−0.427791	−0.358713	−0.083932	−0.401361	−1.390002	−4.107923
2.2	−0.634816	−0.634036	−0.465314	−0.392235	−0.131752	−0.562890	−1.861826	−5.384168
2.3	−0.700613	−0.682588	−0.506343	−0.428900	−0.198311	−0.778577	−2.479509	−7.041482
2.4	−0.771477	−0.735432	−0.551209	−0.469024	−0.289823	−1.065089	−3.286532	−9.192159
2.5	−0.847856	−0.792970	−0.600274	−0.512948	−0.414404	−1.444053	−4.339184	−11.981541
2.6	−0.930242	−0.855640	−0.653938	−0.561048	−0.582641	−1.943519	−5.710341	−15.597795
2.7	−1.019171	−0.923925	−0.712637	−0.613734	−0.808324	−2.599852	−7.494349	−20.284598
2.8	−1.115231	−0.998351	−0.776852	−0.671456	−1.109396	−3.460183	−9.813364	−26.357605
2.9	−1.219065	−1.079497	−0.847112	−0.734707	−1.509177	−4.585580	−12.825577	−34.225845
3.0	−1.331376	−1.167994	−0.923996	−0.804028	−2.037959	−6.055167	−16.735874	−44.419522

Table XI. Ethylene Oxide HCLJ Reduced Virial Coefficients, where $\tau = \varepsilon/k_B T$ and $\varepsilon/k_B = 993.6$ K and $B^*(T) = B(T)/(\frac{2}{3}\pi N_A \sigma^3)$ and $C^*(T) = C(T)/(\frac{2}{3}\pi N_A \sigma^3)^2$ where $\sigma = 0.3458$ nm

τ	$B(\tau)^*$	$\frac{\partial B(\tau)^*}{\partial \tau}$	$\frac{\partial^2 B(\tau)^*}{\partial \tau^2}$	$\frac{\partial^3 B(\tau)^*}{\partial \tau^3}$	$C(\tau)^*$	$\frac{\partial C(\tau)^*}{\partial \tau}$	$\frac{\partial^2 C(\tau)^*}{\partial \tau^2}$	$\frac{\partial^3 C(\tau)^*}{\partial \tau^3}$
0.4	0.043188	−0.124650	−0.115651	0.155723	0.005117	0.003737	0.016323	0.057867
0.5	0.030164	−0.135669	−0.106611	0.041524	0.005581	0.005634	0.021431	0.046289
0.6	0.016069	−0.146225	−0.105380	−0.011117	0.006259	0.008000	0.025821	0.042210
0.7	0.000916	−0.156874	−0.108086	−0.040612	0.007195	0.010790	0.029959	0.040774
0.8	−0.015320	−0.167921	−0.113178	−0.060159	0.008431	0.013989	0.033999	0.040047
0.9	−0.032688	−0.179566	−0.119967	−0.075119	0.010006	0.017587	0.037956	0.038961
1.0	−0.051258	−0.191960	−0.128133	−0.087960	0.011961	0.021574	0.041751	0.036681
1.1	−0.071110	−0.205234	−0.137532	−0.099947	0.014333	0.025927	0.045224	0.032357
1.2	−0.092338	−0.219506	−0.148117	−0.111789	0.017157	0.030600	0.048121	0.024984
1.3	−0.115048	−0.234897	−0.159899	−0.123929	0.020462	0.035520	0.050077	0.013299
1.4	−0.139359	−0.251527	−0.172923	−0.136668	0.024266	0.040568	0.050583	−0.004331
1.5	−0.165399	−0.269525	−0.187260	−0.150233	0.028574	0.045565	0.048943	−0.030031
1.6	−0.193314	−0.289026	−0.203004	−0.164816	0.033369	0.050254	0.044217	−0.066571
1.7	−0.223259	−0.310177	−0.220263	−0.180588	0.038602	0.054264	0.035148	−0.117567
1.8	−0.255409	−0.333134	−0.239166	−0.197713	0.044182	0.057083	0.020066	−0.187729
1.9	−0.289952	−0.358069	−0.259857	−0.216358	0.049956	0.058004	−0.003239	−0.283182
2.0	−0.327095	−0.385170	−0.282494	−0.236694	0.055688	0.056066	−0.037676	−0.411886
2.1	−0.367065	−0.414639	−0.307258	−0.258902	0.061031	0.049972	−0.087065	−0.584167
2.2	−0.410109	−0.446699	−0.334344	−0.283179	0.065487	0.037989	−0.156404	−0.813409
2.3	−0.456499	−0.481592	−0.363969	−0.309733	0.068356	0.017811	−0.252217	−1.116936
2.4	−0.506531	−0.519585	−0.396374	−0.338794	0.068675	−0.013617	−0.383007	−1.517161
2.5	−0.560529	−0.560969	−0.431820	−0.370610	0.065125	−0.060321	−0.559829	−2.043052
2.6	−0.618848	−0.606060	−0.470597	−0.405456	0.055927	−0.127591	−0.797042	−2.732031
2.7	−0.681877	−0.655210	−0.513022	−0.443627	0.038693	−0.222357	−1.113267	−3.632411
2.8	−0.750038	−0.708798	−0.559444	−0.485452	0.010240	−0.353675	−1.532629	−4.806543
2.9	−0.823798	−0.767244	−0.610246	−0.531289	−0.033650	−0.533352	−2.086356	−6.334862
3.0	−0.903664	−0.831007	−0.665849	−0.581530	−0.098550	−0.776758	−2.814833	−8.321105
3.1	−0.990193	−0.900589	−0.726713	−0.636608	−0.191785	−1.103866	−3.770257	−10.899030
3.2	−1.083995	−0.976542	−0.793347	−0.696997	−0.322969	−1.540600	−5.020054	−14.241076
3.3	−1.185734	−1.059470	−0.866307	−0.763217	−0.504669	−2.120564	−6.651281	−18.569521
3.4	−1.296143	−1.150035	−0.946204	−0.835840	−0.753292	−2.887280	−8.776297	−24.170870
3.5	−1.416020	−1.248964	−1.033709	−0.915494	−1.090209	−3.897069	−11.540077	−31.414394
3.6	−1.546241	−1.357055	−1.129560	−1.002869	−1.543213	−5.222761	−15.129629	−40.776046
3.7	−1.687765	−1.475181	−1.234566	−1.098724	−2.148399	−6.958483	−19.786144	−52.869297
3.8	−1.841644	−1.604302	−1.349615	−1.203892	−2.952591	−9.225824	−25.820648	−68.484917
3.9	−2.009027	−1.745471	−1.475685	−1.319289	−4.016467	−12.181786	−33.634194	−88.642308
4.0	−2.191178	−1.899842	−1.613847	−1.445922	−5.418593	−16.029036	−43.743892	−114.655740

Table XII. Trimethyl Gallium HCLJ Reduced Virial Coefficients, where $\tau = \varepsilon/k_B T$ and $\varepsilon/k_B = 1242.35$ K and $B^*(T) = B(T)/(\frac{2}{3}\pi N_A \sigma^3)$ and $C^*(T) = C(T)/(\frac{2}{3}\pi N_A \sigma^3)^2$ where $\sigma = 0.3010$ nm

τ	$B(\tau)^*$	$\frac{\partial B(\tau)^*}{\partial \tau}$	$\frac{\partial^2 B(\tau)^*}{\partial \tau^2}$	$\frac{\partial^3 B(\tau)^*}{\partial \tau^3}$	$C(\tau)^*$	$\frac{\partial C(\tau)^*}{\partial \tau}$	$\frac{\partial^2 C(\tau)^*}{\partial \tau^2}$	$\frac{\partial^3 C(\tau)^*}{\partial \tau^3}$
0.4	−0.006732	−0.243857	−0.193805	0.211305	0.012329	0.032681	0.074860	0.147554
0.5	−0.032060	−0.262522	−0.182225	0.043962	0.015995	0.040874	0.088786	0.134090
0.6	−0.059220	−0.280677	−0.182174	−0.034564	0.020548	0.050418	0.102062	0.132580
0.7	−0.088206	−0.299151	−0.188053	−0.079549	0.026123	0.061291	0.115448	0.135576
0.8	−0.119077	−0.318409	−0.197615	−0.110126	0.032852	0.073521	0.129223	0.139980
0.9	−0.151925	−0.338763	−0.209863	−0.134114	0.040873	0.087150	0.143431	0.144009
1.0	−0.186874	−0.360456	−0.224341	−0.155143	0.050330	0.102218	0.157964	0.146232
1.1	−0.224068	−0.383699	−0.240856	−0.175086	0.061366	0.118745	0.172569	0.145177
1.2	−0.263672	−0.408693	−0.259357	−0.195007	0.074127	0.136721	0.186833	0.139116
1.3	−0.305871	−0.435638	−0.279879	−0.215578	0.088756	0.156081	0.200154	0.125894
1.4	−0.350871	−0.464739	−0.302510	−0.237265	0.105385	0.176692	0.211683	0.102773
1.5	−0.398898	−0.496214	−0.327381	−0.260429	0.124128	0.198320	0.220263	0.066238
1.6	−0.450201	−0.530295	−0.354656	−0.285377	0.145071	0.220595	0.224335	0.011780
1.7	−0.505052	−0.567232	−0.384525	−0.312389	0.168251	0.242968	0.221830	−0.066384
1.8	−0.563751	−0.607294	−0.417211	−0.341739	0.193642	0.264652	0.210023	−0.175655
1.9	−0.626625	−0.650776	−0.452961	−0.373706	0.221122	0.284545	0.185350	−0.325487
2.0	−0.694031	−0.697998	−0.492049	−0.408578	0.250441	0.301140	0.143176	−0.527930
2.1	−0.766361	−0.749307	−0.534783	−0.446663	0.281173	0.312399	0.077504	−0.798310
2.2	−0.844042	−0.805087	−0.581500	−0.488292	0.312654	0.315602	−0.019394	−1.156096
2.3	−0.927541	−0.865753	−0.632572	−0.533823	0.343906	0.307151	−0.157444	−1.625970
2.4	−1.017370	−0.931760	−0.688407	−0.583644	0.373539	0.282322	−0.349357	−2.239188
2.5	−1.114088	−1.003608	−0.749458	−0.638181	0.399621	0.234948	−0.611366	−3.035277
2.6	−1.218305	−1.081842	−0.816216	−0.697898	0.419514	0.157029	−0.964158	−4.064171
2.7	−1.330689	−1.167059	−0.889227	−0.763302	0.429667	0.038221	−1.434043	−5.388883
2.8	−1.451971	−1.259915	−0.969085	−0.834951	0.425355	−0.134786	−2.054421	−7.088869
2.9	−1.582950	−1.361126	−1.056445	−0.913457	0.400339	−0.379078	−2.867634	−9.264228
3.0	−1.724501	−1.471478	−1.152027	−0.999489	0.346442	−0.716512	−3.927277	−12.040986
3.1	−1.877579	−1.591832	−1.256619	−1.093784	0.253010	−1.174987	−5.301118	−15.577704
3.2	−2.043232	−1.723131	−1.371086	−1.197149	0.106236	−1.790037	−7.074740	−20.073764
3.3	−2.222605	−1.866410	−1.496380	−1.310472	−0.111708	−2.606830	−9.356131	−25.779756
3.4	−2.416951	−2.022803	−1.633545	−1.434727	−0.423749	−3.682687	−12.281426	−33.010481
3.5	−2.627644	−2.193553	−1.783726	−1.570986	−0.859281	−5.090246	−16.022117	−42.161250
3.6	−2.856186	−2.380024	−1.948181	−1.720424	−1.455892	−6.921425	−20.794079	−53.728294
3.7	−3.104222	−2.583711	−2.128293	−1.884333	−2.261526	−9.292413	−26.868900	−68.334330
3.8	−3.373556	−2.806254	−2.325577	−2.064134	−3.337216	−12.349920	−34.588067	−86.760588
3.9	−3.666161	−3.049454	−2.541701	−2.261386	−4.760510	−16.279022	−44.380745	−109.986910
4.0	−3.984201	−3.315283	−2.778493	−2.477806	−6.629783	−21.313004	−56.786062	−139.241980

(unitless) form where $B^*(T) = B(T)/(\frac{2}{3}\pi N_A \sigma^3)$ and $C^*(T) = C(T)/(\frac{2}{3}\pi N_A \sigma^3)^2$. Table X spans the reduced temperature range $0.2 \leqslant \tau \leqslant 3.0$ for NF_3 which corresponds to 93 to 1395 K. Tables XI and XII span the reduced temperature range $0.4 \leqslant \tau \leqslant 4.0$ for C_2H_4O and $Ga(CH_4)_4$ which corresponds to 248 to 2482 K and 310 to 3105 K, respectively. These ranges greatly exceed our experimental temperature range; however, the extrapolated virial coefficients are reliable, as demonstrated by our experience with CF_4 and C_2F_6 [1], SF_6 [16], and Trusler et al. experience with C_3H_8 [23]. Of course these molecules will thermally decompose well before reaching these high temperatures.

6. DISCUSSION

A workshop on mass flow control for the semiconductor industry [24] was held in May 2000 at the National Institute of Standards and Technology (NIST). Attending the workshop were 45 scientists and engineers, including representatives from mass flow controller (MFC) manufacturers, semiconductor tool manufacturers, MFC users in the semiconductor and other industries, and representatives from international federal laboratories. The workshop participants identified the need for the thermodynamic and transport properties of semiconductor gases, along with their associated uncertainty levels, that were required to accurately model and calibrate the MFCs; these properties and associated uncertainties were gas density and heat-capacity to 0.1% and the transport properties to 0.5%.

A literature search on the three process gases discussed in this manuscript resulted in only one reference for the second and third virial coefficients of ethylene oxide [25]. The virial coefficients reported here agreed with those of Ref. 25 within their experimental uncertainties. No other published measurements were available. As mentioned before, ideal-gas heat capacities calculated from spectroscopic data and statistical mechanics have, at best, uncertainties on the order of 1%. This is an order of magnitude greater than the 0.1% identified as required. However, our ideal-gas heat capacities have uncertainties typically below 0.1%, thus meeting the requirements of industry.

Only the one small set virial coefficients for ethylene oxide have been published. Estimation methods exist which do a remarkably good job at predicting the virial coefficients of a gas. The correlation of Pitzer and Curl [26] for the second virial coefficient has been used extensively. It was updated by Tsonopoulos [27] in 1974 using a newer and more complete data set. Weber [28] in 1994 further refined the correlation for small polar molecules, and included a estimation method for the third virial coefficient. Until now, the second and third virials estimated using Weber's correlation

were the best "guesses" available. Motivated by the MFC workshop's requirement of densities determined to better than 0.1%, we compared the densities calculated with the HCLJ equation of state for NF_3, C_2H_4O, and $Ga(CH_3)_3$ to the densities calculated using Weber's correlation at each state where the speed of sound was measured.

The densities of nitrogen trifluoride calculated from Weber's correlation had deviations that increased up to 0.3% at 1.0 MPa and 200 K. For both ethylene oxide and trimethyl gallium the densities calculated from Weber's correlation had negative deviations. For C_2H_4O the deviation was -0.5% at 0.9 MPa and 360 K. For $Ga(CH_3)_3$ the deviation was -0.8% at 0.27 MPa and 370 K. When the HCLJ model was extrapolated to temperatures above the experimental temperature ranges, the deviations of the Weber correlation at the highest experimental pressure peaked at 0.8% for NF_3 at 200 K, 1.5% for C_2H_4O at 1000 K, and 2.5% for $Ga(CH_3)_3$ at 800 K. It is impressive that for these three diverse gases, the Weber correlation does predict the density to within 1.0% in our experimental temperature and pressure ranges.

From the work of Gillis and Moldover [14], we believe that the densities calculated from the HCSW potential are within 0.1% of the true densities throughout our experimental temperature and pressure ranges. To support this assumption, we verified that the densities calculated from the HCSW equations of state agreed with those calculated from the HCLJ equations of state within 0.1%.

To make our measurements available in an easy-to-use and timely fashion, a simple database is posted at the URL: http://properties.nist.gov/semiprop. The second and third virial coefficients are tabulated along with their temperature derivatives to allow for interpolation. The ideal-gas heat capacity is tabulated as are estimates for the transport properties. This database will be continually updated as further measurements are acquired.

ACKNOWLEDGMENT

This work has been supported in part by the National Semiconductor Metrology Program.

REFERENCES

1. J. J. Hurly, *Int. J. Thermophys.* **20**:455 (1999).
2. K. A. Gillis, *Int. J. Thermophys.* **15**:821 (1994).
3. K. A. Gillis, A. R. H. Goodwin, and M. R. Moldover, *Rev. Sci. Instrum.* **62**:2213 (1991).
4. H. C. Miller and R. L. Jarry, *J. Phys. Chem.* **10**:1412 (1956).
5. B. A. Younglove, *J. Phys. Chem. Ref. Data*, **11**:S1 (1982).
6. L. A. Weber, *J. Chem. Thermodyn.* **13**:389 (1981).

7. *Nitrogen Trifluoride*; Speciality Gas Data Sheet; Air Products, Allentown, Pennsylvania (1983).
8. J. Gordon and W. F. Giauque, *J. Amer. Chem. Soc.* **71**:2176 (1949).
9. C. Walters and J. Smith, *Chem. Engr. Progr.* 337 (1952).
10. B. J. Zwolinski, A. P. Kudchadker, and G. H. Alani, *Chem. Rev.* **68**:659 (1968).
11. J. Gordon and W. F. Giauque, *J. Amer. Chem. Soc.* **71**:2176 (1949).
12. J. F. Sackman and L. H. Long, *Trans. Faraday Soc.* **54**:1797 (1958).
13. E. E. Grinberg, V. A. Fedorov, E. A. Efremov, and A. A. Efremov, *Russ. J. Phys. Chem.* **47**:918 (1973).
14. K. A. Gillis and M. R. Moldover, *Int. J. Thermophys.* **17**:1305 (1996).
15. J. J. Hurly, *Int. J. Thermophys.* **21**:805 (2000).
16. J. J. Hurly, D. R. Defibaugh, and M. R. Moldover, *Int. J. Thermophys.* **21**:739 (2000).
17. J. J. Hurly, *Int. J. Thermophys.* **21**:185 (2000).
18. T. Kihara, *Rev. Mod. Phys.* **25**:831 (1953).
19. E. A. Mason and T. H. Spurling, *The Virial Equation of State* (Pergamaon Press, Oxford, 1969).
20. R. J. Dulla, J. S. Rowlinson, and W. R. Smith, *Mol. Phys.* **21**:229 (1971).
21. R. F. Boisvert, S. E. Howe, D. K. Kahaner, and J. L. Springmann, *The Guide to Available Mathematical Software*, NISTIR 90-4237 (1990).
22. B. M. Axilrod and E. J. Teller *J. Chem. Phys.* **11**:299 (1943).
23. J. P. M. Trusler, *Int. J. Thermophys.* **18**:635 (1997).
24. B. F. Berg, D. S. Green and G. E. Mattingly, *Semiconductor Measurement Technology: Workshop on Mass Flow Measurement and Control for the Semiconductor industry*, NIST Special Publication 400-101 (U.S. Government Printing Office, Washington, DC, 2001)
25. R. Stryjek, *B. Pol. Acad. Sci. Chem. Sci.* **14**:307 (1966).
26. K. S. Pitzer and R. F. Curl, Jr., *J. Am. Chem. Soc.* **79**:2369 (1957).
27. C. Tsonopoulos, *AIChE. J.* **20**:263 (1974).
28. L. A. Weber, *Int. J. Thermophys.* **15**:49 (1994).
29. M. Chase, JANAF Tables, *J. Phys. Chem. Ref. Data*, **14** (1985).
30. D. Wagman, R. Schumm, V. Parker, R. Nuttall, I. Halow, W. Evans, K. Churney, and S. Bailey, *J. Phys. Chem. Ref. Data.* **2** (1982).
31. *Thermodynamic Properties of Individual Substances*; 4th ed., Vol 2, Elements Carbon, Silicon, Germanium, Tin, Lead, and their Compounds. Pt. 2: Tables (Hemisphere, New York, 1991).
32. M. W. Chase, Jr., *J. Phys. Chem. Ref. Data* **9**:1 (1998).
33. E. F. Westrum, Jr., D. R. Stull, and G. C. Sinke, *The Chemical Thermodynamics of Organic Compounds* (John Wiley, New York, 1969).
34. C. Walters and J. Smith, *Chem. Engr. Progr.* 337 (1952).
35. R. E. Pennington and K. A. Kobe, *Petroleum Refiner* **29**:135 (1950).
36. H. Zeise, *Z. Electrochem.* **47**:595 (1941).
37. *Selected Values of Properties of Chemical Compounds* (Thermodynamics Research Center, Texas A&M University, College Station, Texas, 1984).
38. Y. K. Shaulov and A. M. Mosin, *Russ. J. Phys. Chem.* **50**:319 (1976).